Measurement 283 (2026) 122181

Contents lists available at ScienceDirect

Measurement

journal homepage: www.elsevier.com/locate/measurement

Reliable strain monitoring in asphalt pavement using piezoelectric sensors in bending mode and machine-learning-based calibration

Aliakbar Ghaderiaram [a,*], Ali Golmohammadi [b], Erik Schlangen [a], Mohammad Fotouhi [a]

[a] Delft University of Technology, Delft, the Netherlands
[b] Faculty of Applied Engineering, University of Antwerp, Antwerp, Belgium

ARTICLE INFO

Keywords:
SHM
Piezoelectric
Machine learning
Asphalt
Strain
Bending

ABSTRACT

Ensuring the durability of asphalt pavements is essential for maintaining transportation infrastructure. Structural health monitoring (SHM) supports this by enabling early detection of deterioration. Among SHM techniques, piezoelectric sensors offer real-time strain measurement capabilities, but accurate calibration is crucial for reliable use in applications such as fatigue life monitoring. This study calibrates lead zirconate titanate (PZT) sensors for strain measurement in asphalt pavements by employing machine learning (ML) models to convert voltage signals into accurate strain data under bending loads. In the experimental phase, PZT sensors were tested during four-point bending (4 PB) experiments on Teflon and asphalt beams over a strain range of 15–450 μm/m and loading frequencies from 1–35 Hz. Teflon, with homogeneous mechanical properties, was used to establish baseline strain–voltage relationships in the elastic regime. The resulting dataset was used to analyse sensor behaviour and develop ML-based calibration models. A variety of ML algorithms were evaluated for predictive accuracy, robustness, and consistency. Results showed an approximately linear strain–voltage relationship across both materials, with nonlinearity at higher frequencies attributed to the capacitive nature of the sensors. Ensemble ML models, particularly Extra Trees Regression ($R^2 = 0.978$, RMSE = 24 μm/m) and CatBoost Regression ($R^2 = 0.970$, RMSE = 28 μm/m), achieved the highest accuracy, demonstrating controlled-condition strain calibration. These findings demonstrate that integrating PZT sensors with ML-based calibration can enhance strain measurement reliability in asphalt pavements, providing a foundation for advanced SHM systems aimed at improving pavement performance and service life.

1. Introduction

Asphalt is extensively utilised in civil infrastructures because of its high durability and favourable mechanical properties. However, despite its wide application, it is vulnerable to deterioration over time due to repeated traffic loads and environmental factors such as temperature changes and moisture [1]. Therefore, structural health monitoring (SHM) of asphalt pavements is increasingly important to ensure long-term performance and the safety of transportation infrastructure, especially with the growing demands, aging road networks, and significant economic implications. The use of distributed piezoelectric sensors is a promising SHM method, particularly lead zirconate titanate (PZT) sensors, which can convert mechanical strains into electrical signals, allowing for the detection of micro-cracks, deformation, and damage evolution within the material [2–5]. Piezoelectric sensors are increasingly considered a viable alternative to traditional strain gauges, especially in dynamic loading environments. Compared to conventional resistive gauges, piezoelectric sensors offer several advantages: higher sensitivity, a superior signal-to-noise ratio in high-frequency domains, and passive operation that eliminates the need for external power and reduces system complexity. These features make them particularly attractive for applications involving low strain levels and noisy conditions [6].

In contrast to conventional resistive strain gauges, which are widely used but are inherently sensitive to temperature drift and require an external excitation current, piezoelectric sensors operate passively by generating an electrical charge in response to mechanical deformation, making them particularly suitable for dynamic measurements [6,7]. In addition, piezoelectric sensors typically exhibit a wider usable dynamic strain range compared to strain gauges [54]. Fibre-optic sensing techniques, such as fibre Bragg grating (FBG) sensors, provide high measurement accuracy and immunity to electromagnetic interference [52];

* Corresponding author.
E-mail address: a.ghaderiaram@tudelft.nl (A. Ghaderiaram).

https://doi.org/10.1016/j.measurement.2026.122181
Received 1 December 2025; Received in revised form 3 June 2026; Accepted 5 June 2026
Available online 7 June 2026

however, their high cost, installation complexity, and vulnerability to damage during pavement construction limit their large-scale deployment in asphalt layers [8,9]. MEMS-based approaches typically infer strain indirectly from acceleration or displacement measurements, introducing additional modelling uncertainty associated with numerical integration and kinematic assumptions [10,53]. Consequently, PZT sensors represent a practical compromise between sensitivity, robustness, and applicability for laboratory-validated dynamic strain monitoring in asphalt pavements.

Recent research has explored the integration of PZT sensors with machine learning (ML) models to improve the capabilities of SHM systems [11–15]. ML models can effectively interpret electromechanical impedance (EMI) data collected from PZT sensors, enabling automated detection, classification, and prediction of damage progression. These data-driven approaches allow for the identification of subtle patterns and anomalies that may not be easily captured through traditional analysis. Moreover, physics-informed ML methods, such as Gaussian process regression, have been used to enhance model robustness and adaptability under varying environmental and loading conditions [16]. Such hybrid systems offer a scalable and efficient framework for real-time monitoring, with the potential for predictive maintenance and long-term infrastructure resilience. While existing literature has primarily focused on using ML models for tasks such as optimising asphalt mix designs [17–19] or classifying pavement damage types [20–22], limited attention has been given to the application of ML for real-time pavement monitoring through sensor data interpretation. Han et al. [11] introduced a field-validated deep learning framework for in-situ concrete strength monitoring using piezoelectric-based EMI data. To overcome the limitations of previous studies that relied on homogeneous datasets, they constructed a comprehensive database comprising over 100 sensors and 28 different mix designs. A novel one-dimensional convolutional neural network incorporating a baseline correction mechanism was developed, achieving a coefficient of determination (R^2) of 0.96 and a mean prediction error of 2.68 MPa. The model was successfully validated on actual highway pavement projects, demonstrating strong reliability under real-world conditions. Furthermore, the use of transfer learning improved the model's adaptability to different sensor types and mix designs, offering a scalable and generalisable solution for SHM using piezoelectric sensors. Wang et al. [12] reviewed recent progress in intelligent compaction technologies, highlighting the role of smart sensors, particularly PZT sensors, in monitoring asphalt pavement conditions. The study emphasised the potential of integrating PZT sensing with machine learning to improve real-time assessment of compaction quality and structural integrity. The paper identifies several key gaps including limited integrating data from multiple sensor types, lack of real-world experimental data, underutilisation of advanced machine learning in practical applications, and challenges related to operational robustness in real-world conditions.

Despite the potential of piezoelectric sensors, achieving accurate calibration for asphalt pavement applications remains a significant challenge. The calibration here refers to the process of establishing a reliable and accurate relationship between the sensor output (e.g., voltage or charge generated by the piezoelectric sensor) and the strain quantity being measured. Strain measurement in asphalt pavements using PZT sensors is particularly challenging. This is because asphalt experiences a broad spectrum of strain values and loading frequencies due to traffic and environmental variations [23–25]. Low-strain measurement comes with low signal-to-noise conditions, and the frequency-dependent sensor behaviour which can lead to different voltage outputs for identical strain levels, complicating data interpretation. As a result, reliable use of piezoelectric sensors in asphalt requires the development of experimentally validated, geometry-specific signal–strain relationships that account for strain levels, frequency effects, and bonding conditions. Therefore, rather than explicitly modelling these complexities, this study adopts a data-driven approach where experimentally collected sensor data from PZTs attached to asphalt under controlled loading conditions and ML techniques are used to learn the relationship between sensor output and applied strain across 1–35 Hz. A key challenge lies in evaluating the reliability of ML methods with varying levels of complexity to develop computationally efficient and accurate signal processing strategies. Specifically, there is a need to convert piezoelectric sensor outputs into meaningful strain measurements and to systematically compare multiple ML algorithms to enhance the calibration process. Accordingly, this paper aims to investigate the use of different ML models to interpret voltage signals from PZT sensors into precise strain data in asphalt structures under bending loads. More specifically, ML models with different levels of complexities were systematically evaluated for their predictive accuracy, robustness, and consistency using a range of regression performance metrics, including R^2, MAE, MSE, and RMSE. Such an approach could enable early detection of dynamic strain induced events, thereby supporting smarter maintenance and longer service life for asphalt pavements. Although fatigue assessment is not the focus of this work, the methods developed here provide a foundation for future research in that direction. The novelty of this work lies in establishing and experimentally validating a systematic calibration framework for PZT-based strain sensing in viscoelastic asphalt under bending conditions. The results provide key insight into extending piezoelectric strain monitoring from uniaxial, homogeneous systems to complex flexural and viscoelastic environments. By integrating cross-material validation, attachment strategy assessment, and multi-metric benchmarking of different machine learning algorithms, the study delivers reproducible guidelines for reliable dynamic strain monitoring. It highlights the necessity and effectiveness of data-driven calibration approaches, evaluates the performance of various ML models, identifies limitations in strain-transfer mechanisms (e.g., TEA under flexural loading), and quantifies the influence of loading frequency and strain amplitude on measurement reliability. Ultimately, these findings offer a route towards more accurate, real-time SHM that can inform maintenance decisions and improve the durability of road infrastructures.

2. Working principles: piezoelectricity

Piezoelectricity is the property of certain materials to generate an electric charge in response to applied mechanical strain, arising from their non-centrosymmetric crystal structure, which produces a net electric dipole moment upon deformation [26]. In sensor applications, including the present study, the direct piezoelectric effect is utilised, whereby mechanical strain induces electrical displacement and generates a measurable voltage output [2]. Under linear constitutive assumptions, the coupled electromechanical behaviour of a piezoelectric material can be expressed as Eq. (1) [26].

$$D_m = \varepsilon_{mn}E_n + d_{mkl}T_{kl} \tag{1}$$

where D is the electric displacement component, E is the electric field, T the mechanical stress tensor, ε the permittivity at constant stress, and d the piezoelectric coefficient tensor. The indices $m, n, k, l \in \{1, 2, 3\}$ denote Cartesian components, and repeated indices imply summation according to the Einstein convention. Since the sensors operate passively under open-circuit conditions without an externally applied electric field, the electric field contribution $\varepsilon_{mn}E_n$ can be neglected [6]. Under this assumption, the electrical displacement is governed primarily by the piezoelectric coupling term $d_{mkl}T_{kl}$. Consequently, within the linear operating regime, the generated voltage V_{PZT} is directly proportional to the applied mechanical stress. Electrically, a piezoelectric element can be represented by an equivalent circuit, formalised in [27] as Equation (2).

$$v_{PZT(t)} = \frac{A}{C} e^{\frac{-t}{\tau}} \int_0^T e^{\frac{t}{\tau}} \frac{dD_3}{dt} dt \tag{2}$$

where A is the electrode area, C the inherent capacitance, R the equivalent resistance of the sensor–measurement system, and $\tau = RC$ the system time constant. This expression shows that V_{PZT} depends on the rate of electrical displacement and the RC dynamics of the system, introducing a frequency-dependent nonlinearity in the voltage–strain relationship.

Mapping the bending-induced strain field to the corresponding electrical displacement is further complicated by the anisotropic and layered nature of the system. The substrate, piezoelectric layer, and adhesive each have distinct mechanical properties, and strain transfer is affected by both geometry and bonding conditions [6]. These coupled electromechanical effects make it challenging to obtain an accurate analytical solution for V_{PZT} under varying loading conditions. Given these complexities, this study adopts a data-driven calibration approach, training machine-learning models on experimental strain–voltage data to learn the combined mechanical–electrical behaviour without requiring an explicit closed-form model.

3. Materials and methods

A series of 4 PB tests were conducted using piezoelectric sensors attached to Teflon samples to generate a dataset. This test method was chosen because the sample experiences a fairly uniform strain between two internal supports that can help for a more accurate comparison. These tests were performed under strain-controlled conditions at a constant temperature of 20 °C (climate chamber) to minimise temperature-induced variability in asphalt viscoelastic response and to isolate the effects of strain amplitude, loading frequency, and sensor behaviour for model training. After acquiring the data, piezoelectric sensor outputs were integrated with strain measurements obtained from a linear variable differential transformer (LVDT) in the testing machine as a reference. The LVDT measures the vertical mid-span deflection of the beam, from which the tensile strain at the bottom fibre was calculated using standard four-point bending beam theory based on the known specimen geometry and loading configuration. The testing system is factory-calibrated, and according to manufacturer specifications, the LVDT displacement resolution is on the order of micrometres. Based on this resolution and the beam dimensions, the corresponding strain uncertainty is estimated to be within the typical microstrain range of laboratory 4 PB measurements, which is small compared to the strain amplitudes investigated in this study. Using this dataset, various well-known ML models were trained to establish a predictive relationship between piezoelectric sensor output and applied strain. This study evaluates a wide range of regression models, including linear models (linear, polynomial, Ridge, Lasso, ElasticNet) [28], discriminative-based models (SVR) [29], ensemble models (Random Forest, Gradient Boosting, CatBoost, Bagging Regression) [30], instance-based model (K-nearest neighbour) [31], tree based model (decision tree) [32], and neural networks [33,34]. Table 1 provides an overview of all models considered, their general category, a brief description of their working principles, and relevant references. The final tabular dataset used for ML training consisted of approximately 500 samples, generated from 10 strain levels and 10 loading frequencies with at least five repetitions per condition. The dataset was divided into 80% training data and 20% testing data. Although the input space is low-dimensional (voltage and frequency), a broad set of regression models was considered to benchmark different modelling families and identify robust candidates for strain calibration under varying operating conditions.

These models were selected for their proven effectiveness in regression tasks and their complementary modelling capacities. Once trained, these models become adaptable to any type of material (including anisotropic and heterogeneous) because the relationship between strain and voltage amplitude remains constant across different material substrates. To validate this adaptability, the trained models were tested on asphalt beams at certain strain levels and frequencies. Asphalt was not used for initial model training due to its complex mechanical behaviour as a heterogeneous material, which can be unpredictable, leading to sudden failure and potential sensor damage. Additionally, asphalt's variability might not provide a stable dataset for effective ML model training. Fig. 1 presents an overview of the experimental and analytical framework used in this research as well as offering potential future studies.

Table 1
Overview of ML models used in this study.

Category	Model	Brief Definition	Ref
Linear (Regularized)	Ridge Regression	Estimates regression coefficients with L2 regularization, effective when predictors are highly correlated.	[35]
	Lasso Regression	Performs variable selection and L1 regularization to enhance prediction accuracy and interpretability.	[36]
	Elastic Net	Combines L1 and L2 penalties of Lasso and Ridge; typically, more accurate in reconstruction.	[37]
	Polynomial Regression	Models the relationship between variables as a polynomial function of the predictors.	[38]
Discriminative-based models	SVR	Extends SVM to regression by finding the optimal tube around the function to minimize prediction error.	[39]
Instance-Based	KNN Regression	Predicts outcome based on average of nearest neighbours' outputs in feature space.	[40]
Deep Learning	Neural Network Regression	Predicts continuous values using interconnected layers optimized to minimize prediction error.	[41]
Tree-Based	Decision Tree Regression	Predicts values by recursively splitting data based on feature thresholds.	[42]
Ensemble models	Random Forest Regression	Averages predictions from multiple decision trees built on bootstrap samples.	[42]
	Extra Trees Regression	Builds trees with random feature subsets and split thresholds for robust, fast regression.	[43]
	Bagging Regression	Aggregates predictions from multiple models trained on bootstrap samples to reduce variance.	[44]
	Gradient Boosting Regression	Sequentially trains weak learners to correct residual errors, producing a strong final model.	[45]

In this study, trained models were compared based on their predictive accuracy and consistency using several widely accepted regression performance metrics, including the coefficient of determination (R^2), mean absolute error (MAE), mean squared error (MSE), and root mean squared error (RMSE). Quantile and expectile loss functions were also applied to provide a more nuanced evaluation of predictive behaviour, especially in cases with non-normal error distributions.

To ensure the robustness and generalisation of the models, k-fold cross-validation ($k = 5$) was employed [46]. The dataset was derived from cyclic tests, where each loading condition produced multiple consecutive measurements. A randomized k-fold cross-validation ($k = 5$) strategy was employed, meaning that samples from the same test condition may appear in both training and validation sets. Due to the correlated nature of cyclic data, this can lead to slightly optimistic performance estimates. More rigorous validation strategies, such as grouped or block-based splitting, may provide a stricter assessment of model generalisation and will be considered in future work. This strategy partitions the training data into five subsets, iteratively training the model on four subsets and validating on the remaining one. This helps mitigate overfitting and produces a more reliable estimate of model performance across unseen data. The magnitude of any potential performance overestimation cannot be quantified from the available data and validation framework.

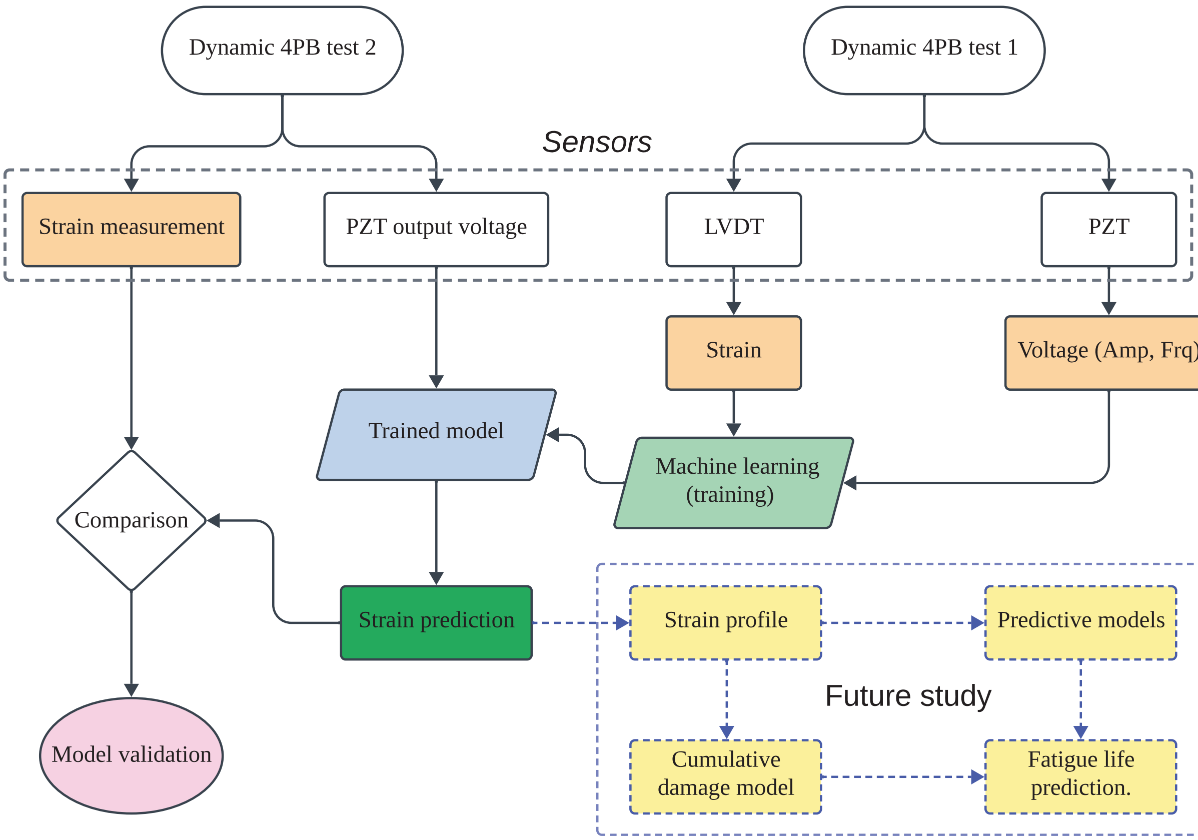

Fig. 1. The framework of the current study.

An essential step in developing ML models is the optimisation of hyperparameters, settings that influence the model's learning process and structure but are not learned directly from the data. Inappropriate hyperparameter choices can significantly reduce a model's performance,

Table 2
Summary of the hyperparameter grids.

Model	Hyperparameters (Before Tuning)	Optimized Hyperparameters (After Tuning)
Linear Regression	No parameter	No parameter
Ridge Regression	'alpha': [0, …, 20]	'alpha': 15.56
Lasso Regression	'alpha': [0, …, 20]	'alpha': 8.69
ElasticNet Regression	'alpha': [0.01, …, 20], 'l1_ratio': [0.01, …, 20]	'alpha': 0.27 'l1_ratio': 0.11
Polynomial Regression	'polynomialfeatures__degree': [1–5]	'polynomialfeatures__degree': 4
SVR	'C': [0.1, 1, …, 10000], 'epsilon': [0.01, 0.1, 0.2, 0.5, 1], 'kernel': ['rbf'], 'degree': [2–4], 'gamma': [0.1, 1, 2, 5, 10]	'C': 5000 'degree': 2 'epsilon': 0.01 'gamma': 0.1 'kernel': 'rbf'
K-Nearest Neighbors	'n_neighbors': [1, …, 200], 'weights': ['uniform', 'distance'], 'algorithm': ['auto', 'ball_tree', 'kd_tree', 'brute'], 'leaf_size': [1, 3, 5, 7, …, 53], 'p': [1,2]	'algorithm': 'auto' 'leaf_size': 5 'metric': 'chebyshev' 'n_neighbors': 2 'p': 1 'weights': 'distance'
Random Forest	'n_estimators': [50, …, 2000], 'max_features': ['auto', 'sqrt'], 'max_depth': [10, …, 100, None], 'min_samples_split': [2,5,9], 'min_samples_leaf': [1,2,4,6], 'bootstrap': [True, False]	'n_estimators': 500 'max_features': 'auto' 'max_depth': None 'min_samples_leaf': 1 'min_samples_split': 2 'bootstrap': True
Decision Tree	'criterion': ['squared_error', 'friedman_mse', 'mae'], 'splitter': ['best', 'random'], 'max_depth': [None, 10, …, 500], 'min_samples_split': [2,5,9], 'min_samples_leaf': [1,2,4,7], 'max_features': ['auto', 'sqrt', 'log2', None], 'max_leaf_nodes': [None, 10, 20], 'min_impurity_decrease': [0.0, 0.001, 0.1, 0.2], 'min_weight_fraction_leaf': [0.0, 0.001, 0.1, 0.2]	'criterion':'friedman_mse''max_depth': 500'max_features': None'max_leaf_nodes': None'min_impurity_decrease': 0.2'min_samples_leaf': 1'min_samples_split': 2'min_weight_fraction_leaf': 0.001'splitter':'random'
Gradient Boosting Regression	'n_estimators': [50, …, 500], 'max_depth': [3–5]	'n_estimators': 200 'max_depth': 3
Extra Trees Regression	'n_estimators': [48], 'max_depth': [None, 10, 20], 'min_samples_split': [2,5,9], 'bootstrap': [True, False], 'warm_start': [True, False]	bootstrap': False'max_depth': None'min_samples_split': 2'n_estimators': 100'warm_start': True
Neural Network	'hidden_layer_sizes': [(10,), (10,10), …], 'alpha': [0.0001, 0.001, 0.01, 0.1, 1, 2], 'max_iter': [1000]	'alpha': 1'hidden_layer_sizes': (10, 10, 10, 10, 10)'max_iter': 1000
Bagging Regression	'n_estimators': [2, …, 200], 'max_samples': [0.5, …, 1.0], 'max_features': [0.1, …, 5]	'max_features': 1.0'max_samples': 0.94'n_estimators': 18
CatBoost Regressor	'iterations': [2, 4, …, 100], 'learning_rate': [0.01, 0.1, 0.2], 'depth': [6,7,9,14], 'l2_leaf_reg': [1,3,5,6,8,9]	'depth': 6'iterations': 94'l2_leaf_reg': 1'learning_rate': 0.2

even if the model itself is robust. To address this, the study employed the GridSearchCV algorithm [47], a widely used method that performs an exhaustive search over a predefined hyperparameter grid. This algorithm systematically evaluates all possible combinations of specified hyperparameter values using cross-validation. The primary objective of this optimisation process was to identify the set of hyperparameters for each model that minimised RMSE. To ensure fair and effective comparison between models, hyperparameter tuning was conducted using a grid search strategy with 5-fold cross-validation. Each model was evaluated across a comprehensive parameter space to capture optimal configurations, particularly for nonlinear and ensemble-based models. A full summary of the hyperparameter search grids and the corresponding best-performing values for each algorithm is provided in Table 2. This allows transparent benchmarking and facilitates reproducibility for future studies using similar data-driven sensor calibration pipelines.

Although some tree-based models resulted in large or unconstrained depths, overfitting was mitigated through 5-fold cross-validation and evaluation across validation folds. Ensemble methods such as Extra Trees reduce variance by averaging multiple decorrelated trees, which improves generalisation. Given the low-dimensional input space (voltage and frequency), the effective complexity of the learned relationship remains limited. The consistent performance observed across validation folds suggests that the models capture the underlying relationship rather than memorising individual data points.

To further enhance the interpretability of model outputs and ensure transparency in predictions, SHAP (SHapley Additive exPlanations) analysis was employed [22]. This approach helps quantify the individual contributions of input features, such as voltage and frequency, to the model's predicted strain values, thereby supporting more trustworthy ML-based calibration strategies.

For this study, an asphalt concrete (AC) slab was manufactured using a 16 Bin/Base 35/50 mixture at the Laboratorium Ontwikkeling Wegenbouw (Dura Vermeer) in Eemnes, Netherlands. This specific mixture contained a minimum of 65% Reclaimed Asphalt Pavement (RAP) and was designed with a target binder content of 4.3% by mass, utilising a 20 mm penetration grade binder. The asphalt mixture was produced at a temperature of 165–170 °C to ensure proper binder activation and homogeneity. A total of eight asphalt beams were fabricated for the 4 PB tests, each measuring 400 × 50 × 50 mm. Additionally, a Teflon sample with the same dimensions was prepared to conduct preliminary tests without the risk of damaging the piezoelectric sensor. A piezoelectric sensor with a 50 × 30 mm sensing area, sourced from a DuraAct patch transducer provided by Physik Instrumente (P-876.A12), was selected for strain measurement (Fig. 2(c)). The sensor's technical detail is presented in Table 3. The sensor was securely attached to the bottom centre of both the Teflon and asphalt samples using a transparent double-sided PET-based adhesive tape with rubber adhesive and an approximate thickness of 0.1 mm. The same bonding procedure

Table 3
Piezoelectric sensors (P-876.A12) properties.

Property	Qty	Unit
Min. lateral contraction	650	*μm/m*
Min. bending radius	20	*mm*
Poisson ratio	0.35	
Young's moduli $E_1 = E_2$	63E9	Nm^{-2}
Young's modulus	16.4E9	Nm^{-2}
$d_{31} = d_{32}$	−175E-12	CN^{-1}
d_{33}	395E-12	CN^{-1}
Electrical capacitance	90	*nF*
Piezo ceramic	PIC255	
Dimensions	61 × 35 × 0.5	*mm*

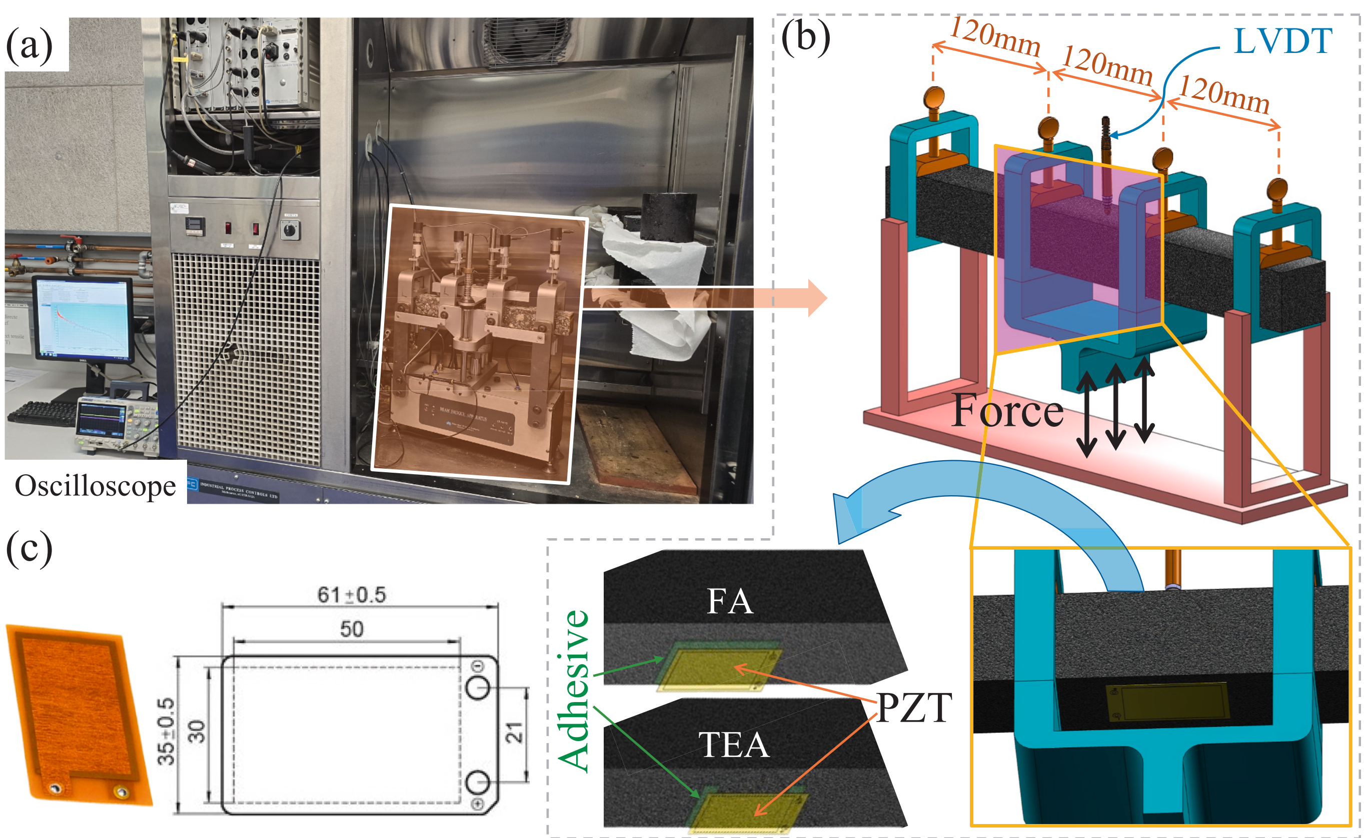

Fig. 2. Illustration of the experimental setup: (a) 4 PB machine with the asphalt sample and attached piezoelectric sensor, alongside the oscilloscope used for voltage measurement, (b) schematic representation of clamp positioning and the two sensor attachment configurations and (c) dimensions of the PZT sensor used in this study.

was consistently applied to all specimens to minimise variability in strain transfer. The influence of bonding conditions on piezoelectric strain transfer has been investigated in our previous work under tensile loading conditions [6]; however, a quantitative strain-transfer analysis of the adhesive layer was beyond the scope of the present study. The sensor was also fastened with duct tape to further enhance stability and prevent displacement during testing. Special attention was given to ensuring accurate electrode positioning and electrical contact connections to maintain signal integrity. Fig. 2(a) and Fig. 2(b) illustrates the test setup and samples with the attached piezoelectric sensors.

Before starting the main tests, a preliminary experiment was carried out to figure out the influence of the PZT sensor attachment method on its measurement accuracy, to inform future studies. For this purpose, two attachment configurations were investigated. In the first configuration, the PZT sensor was fully attached to the substrate, ensuring complete surface contact. In the second configuration, the sensor was only partially (at two ends) attached to the substrate, as illustrated in Fig. 2(b). This TEA configuration was included based on previous findings in uniaxial strain measurements on steel substrates, where TEA demonstrated a key advantage over FA configurations: it made the sensor's response less sensitive to the substrate's Poisson ratio [6]. By reducing the influence of transverse strain components, TEA enables a more direct and consistent relationship between axial strain and sensor output. Extending this concept to bending scenarios, the current study aimed to explore whether similar benefits could be observed when applying TEA to piezoelectric sensors under flexural loading conditions. Comparing both configurations provides insight into the robustness and generalisability of the TEA approach for dynamic strain sensing in different materials. The TEA configuration was included to evaluate whether attachment strategies previously shown to reduce transverse strain sensitivity under uniaxial loading could be transferred to bending conditions, rather than as a representation of in-service pavement stress states.

Following this, a series of 4 PB experiments were conducted to assess the sensor's performance. These trials spanned a frequency range of 1–35 Hz and strain levels of 15–450 μm/m, selected to cover a broad range of dynamic laboratory conditions relevant to asphalt pavement response reported in previous pavement fatigue and strain-monitoring studies [48,49]. The 4 PB setup included loading clamps designed to allow both upward and downward movement, as schematically illustrated in Fig. 2(b). The setup was equipped with a LVDT positioned at the midpoint to measure deformation. The measured deformation was then converted into strain, serving as a reference for model training. Asphalt mixtures may exhibit bimodular behaviour, with different stiffness in tension and compression, leading to asymmetric mechanical responses under four-point bending. Previous studies have shown that

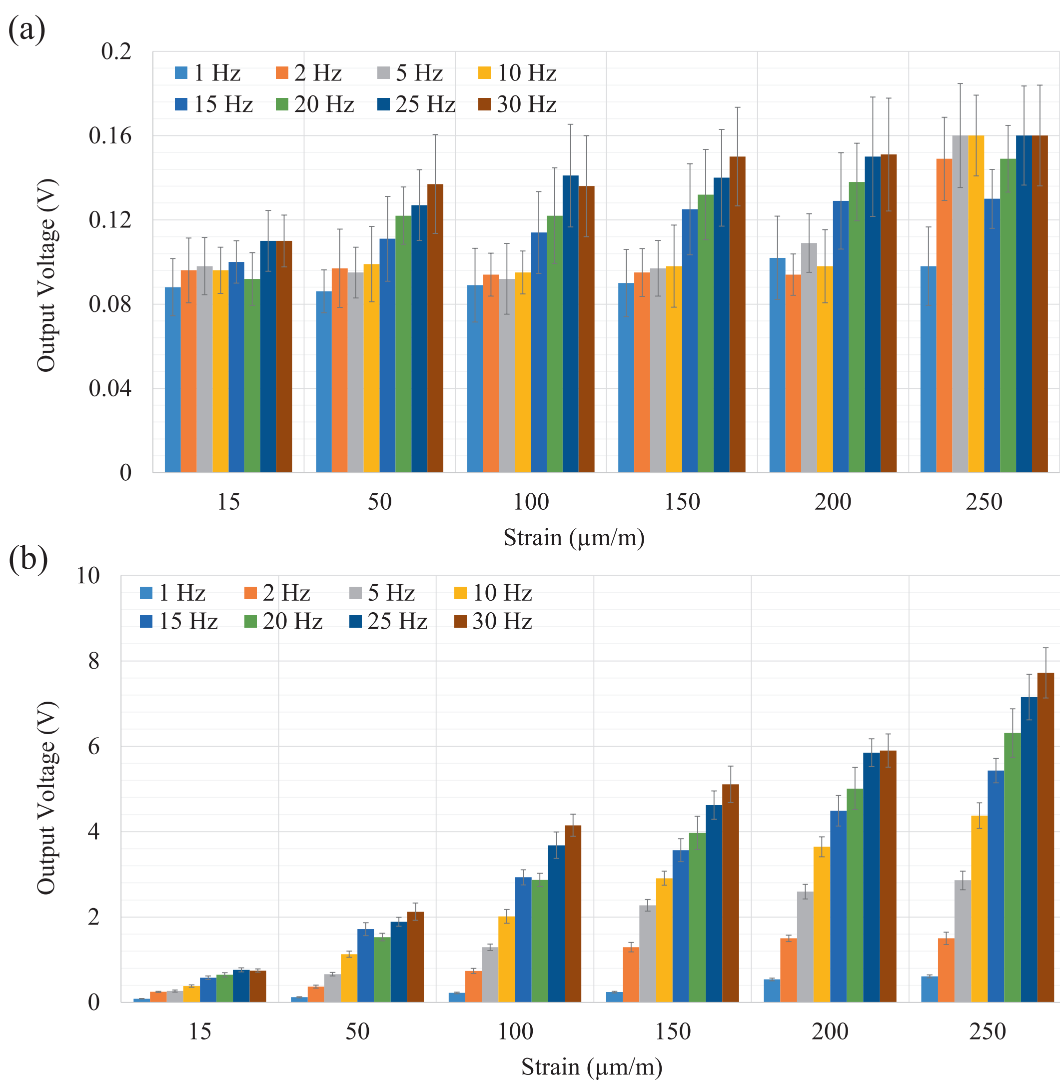

Fig. 3. The PZT sensor output peak-to-peak voltage as a function of strain in a range of different frequencies for two different attachment configurations, (a) TEA and (b) FA.

such bimodular effects can influence strain interpretation and modulus estimation in both indirect tensile and four-point bending tests, particularly under cyclic loading conditions. In the present study, the strain derived from mid-span deflection is therefore treated as an effective global reference rather than an exact bottom-surface tensile strain. The machine-learning-based calibration does not rely on an explicit analytical strain–deflection relationship; instead, it learns an empirical mapping between the PZT sensor output and the bending-induced response, implicitly accounting for potential bimodular effects [50,51]. As shown in Fig. 2(a) a digital oscilloscope was utilized to capture the PZT sensor's output.

After hyperparameter tuning and model training, the selected algorithms were evaluated on the test dataset using performance metrics. The following section presents the comparative results and their implications for piezoelectric sensor calibration under dynamic loading.

4. Results and Discussions

Fig. 3(a) and (b) present the primary test results evaluating the impact of different sensor attachment methods. In the case of the TEA method, as shown in Fig. 3(a), the PZT sensor failed to generate a significant voltage response, suggesting poor signal transmission and inadequate mechanical coupling, but the measurement error is also considerably high. In contrast, the FA configuration exhibits more reliable behaviour, characterised by lower variability and an approximately linear relationship between output voltage and strain, as depicted in Fig. 3(b). This linear response aligns with the fundamental piezoelectric governing equation (Equation (1), which predicts a proportional relationship between mechanical stress and electrical displacement. However, it is worth noting that the degree of linearity diminishes with increasing frequency due to rate-dependent effects. One likely reason for the poor performance of the TEA configuration is the presence of a gap between the sensor and the substrate (Fig. 2(b)), which prevents the

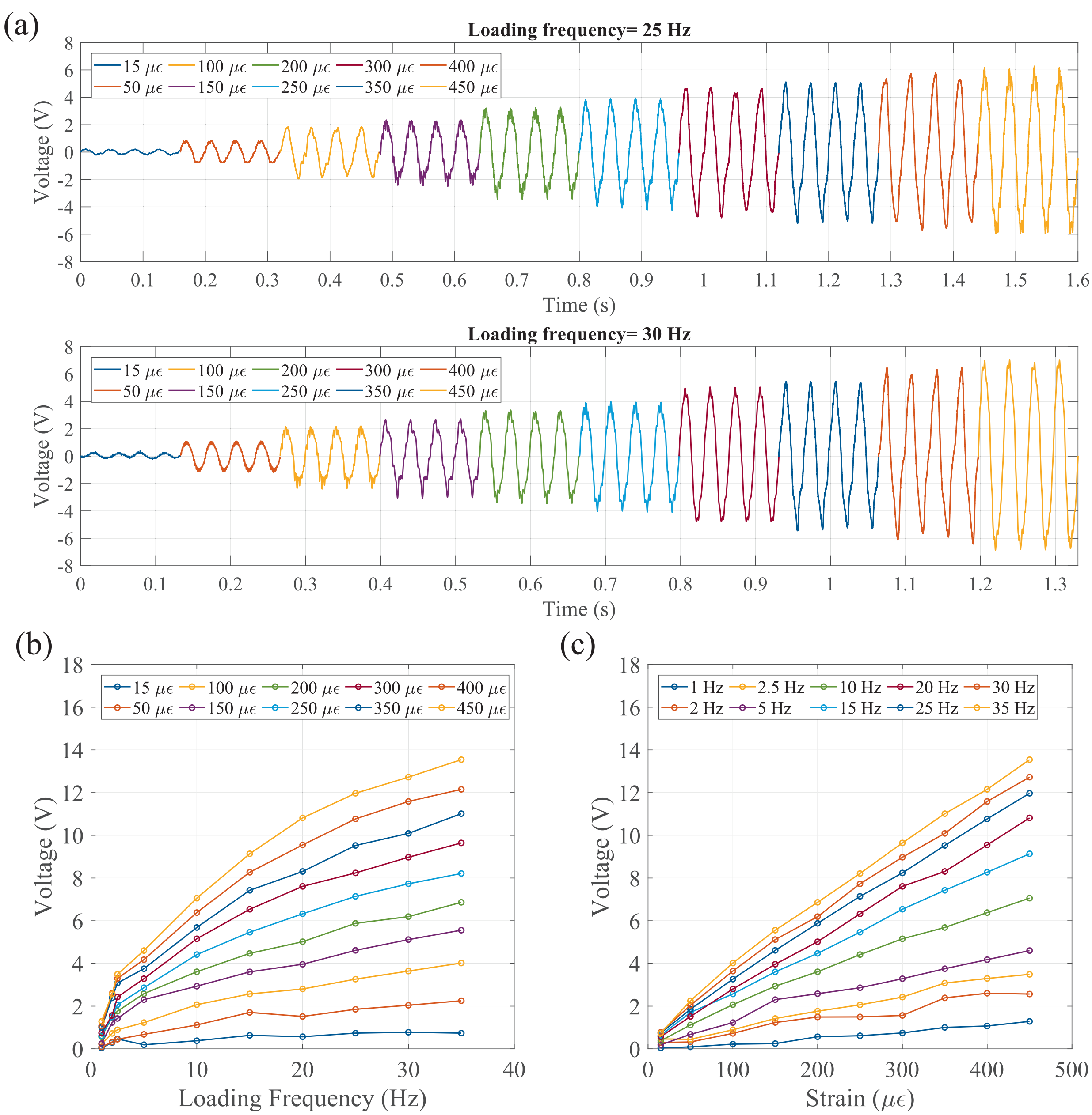

Fig. 4. Piezoelectric sensor output voltage (a) for loading frequency 25 Hz and 30 Hz, (b) peak-to-peak voltage responses for different strain levels at various frequencies, (c) peak-to-peak voltage responses for different frequencies at various strain levels.

sensor from accurately following the substrate's bending and applied strain. Based on these findings, the FA configuration demonstrated superior performance and was therefore selected for all subsequent experiments.

Although the TEA configuration does not reflect the multi-axial stress state of asphalt pavements, its poor performance under bending provides useful evidence that partial attachment is unsuitable for reliable strain calibration in flexural SHM applications. This negative result helps prevent inappropriate transfer of TEA-based attachment strategies to bending scenarios and reinforces the necessity of fully attached configurations for asphalt pavement strain monitoring. The comparison between TEA and FA configurations was intended to evaluate the transferability of attachment strategies across different loading conditions. The results indicate that configurations effective under uniaxial loading may not be suitable for bending, highlighting the need for bending-specific attachment designs. Optimised partially attached configurations (e.g., segmented bonding) may therefore be explored in future work.

Fig. 4(a) illustrates examples of the voltage output of the piezoelectric sensor over time during selected 4 PB tests on the Teflon beam, under varying strain levels and 25 and 30 Hz loading frequencies. The figure highlights representative trends across low, medium, and high strain and high frequency conditions.

The waveforms confirm that the piezoelectric sensor reliably responds to the applied mechanical excitation by generating voltage that closely follow the cyclic strain input. However, certain deviations from ideal sinusoidal behaviour, particularly noticeable in low-amplitude signals, are observed as high-frequency perturbations superimposed on the main waveform. These fluctuations are likely caused by mechanical inconsistencies or transient disturbances in the 4 PB setup, including noise introduced by the pneumatic actuator's control system. In order to verify that the bending experiments remained within the elastic region, stress–strain relationships were obtained for Teflon specimen as shown in Fig. 5, for four representative frequencies exhibiting linear stress–-strain behaviour within the applied strain range. This confirms that all calibration tests were carried out in the elastic domain, avoiding nonlinear or damage-induced effects.

Interestingly, these high-frequency components are more prominent in the signals with a lower voltage amplitude, where the signal-to-noise ratio (SNR) is inherently low, making the system more sensitive to external disturbances. At higher strain levels, where the sensor output voltage is larger, these perturbations become less noticeable due to the improved SNR, effectively masking the noise contributions. This behaviour highlights the importance of considering both sensor output magnitude and mechanical system stability in the interpretation and calibration of piezoelectric responses.

Fig. 4(b) presents the output voltage of the piezoelectric sensors as a function of loading frequency for different applied strain levels. The voltages were calculated as the mean of repetitive peak-to-peak measurements over more than 50 cycles, with an associated measurement error of less than 11%, ensuring a reliable trend observation.

The results reveal a nonlinear relationship between output voltage and loading frequency, especially at higher strain levels and frequencies, while Fig. 4(c) demonstrates that the relation between output voltage and strain level at the same loading frequency is mostly linear. The nonlinearity of loading frequency dependency can be attributed to the capacitive nature of the piezoelectric sensor, as described by the equivalent circuit model outlined in Equation (2). According to the equivalent model, the piezoelectric sensor behaves electrically like a capacitor, where the generated charge is influenced by the strain input, and the output voltage is dependent on the effective impedance of the sensor and connected electronics.

Since the measurements are performed in a steady-state regime, the observed nonlinearity is not due to transient behaviour, but rather to the frequency-dependent impedance of the capacitive element. As the excitation frequency increases, the capacitive reactance decreases, leading to a reduction in output voltage for a given generated charge, knowing that the connected electronic impedance is the oscilloscope's input impedance of 1 MΩ. This explains the voltage attenuation observed at higher frequencies, consistent with the sensor's equivalent circuit behaviour predictions.

These findings reinforce the necessity of accounting for both mechanical and electrical system characteristics when interpreting piezoelectric sensor outputs, particularly in dynamic SHM applications. In addition to the complexity arising from multi-layer mechanical behaviour and non-uniform strain distributions within the substrate and

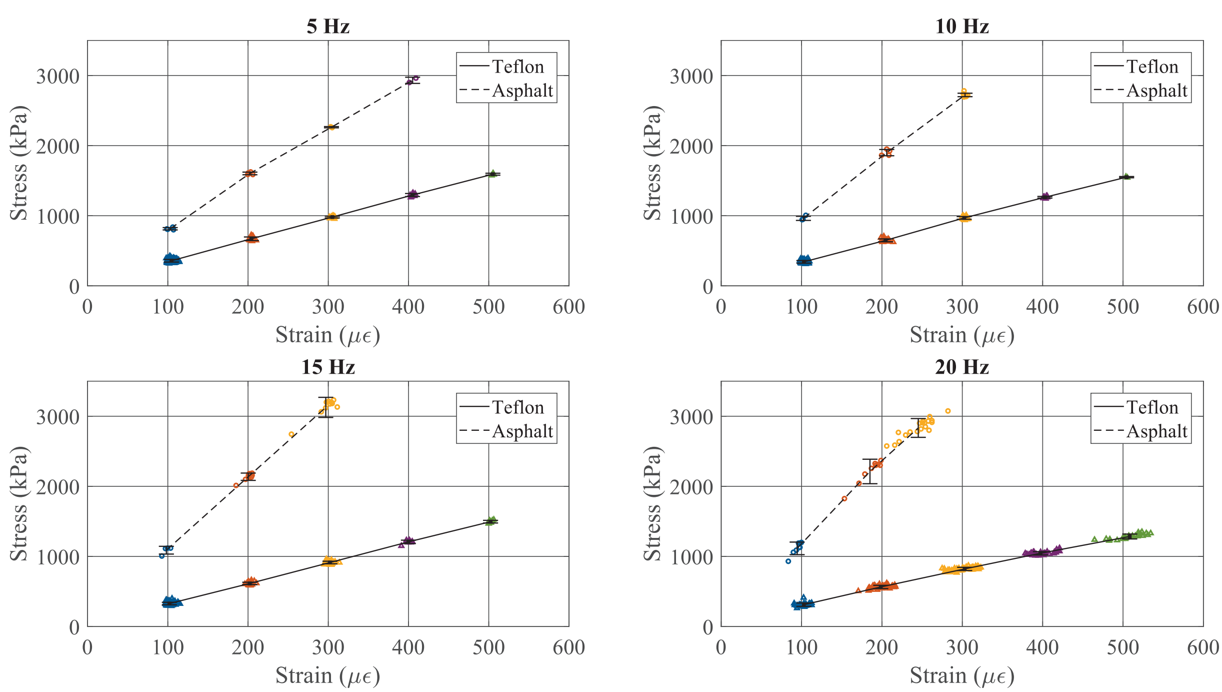

Fig. 5. Stress–strain relationships of cyclic 4 PB tests for both Teflon and asphalt specimens.

adhesive layers, the frequency-dependent electrical response introduces further modelling challenges. These complexities reduce the reliability of purely analytical solutions. Consequently, ML models offer a powerful alternative by learning the intricate interactions between mechanical strain, electrical impedance, and sensor output, thereby improving the accuracy and robustness of signal interpretation under realistic operating conditions.

To evaluate the predictive capability of the proposed calibration framework, a range of ML models were developed and assessed using the experimental dataset. Fig. 6(a) and Fig. 6(b) present a unified summary of the performance metrics for all models considered. The evaluation criteria include RMSE, coefficient of determination R^2, MAE, Quantile Loss, and Expectile Loss.

From the results shown in Fig. 6(a), Extra Trees Regression, SVR, Gradient Boosting Regression, Bagging Regression, Neural Network, and CatBoost Regression models demonstrate superior performance, achieving high R^2 values and low error levels. Among these, the Extra Trees Regression model stands out with the lowest RMSE (24.080) and the highest R^2 (0.978), indicating strong predictive accuracy. Furthermore, an analysis of Quantile Loss and Expectile Loss, metrics that offer additional insights into model robustness, confirms that Extra Trees Regression, CatBoost Regression, and Gradient Boosting Regression achieve the best performance (see Fig. 6(b)). These findings suggest the potential suitability of ensemble-based models within the adopted laboratory validation framework for capturing the complex, nonlinear relationships present in the dataset.

To improve the interpretability and trustworthiness of the ML models, SHAP analysis was conducted [22]. SHAP values quantify the contribution of each feature, voltage and frequency, in this case, to the final model prediction. As shown in Fig. 7, the SHAP visualisations highlight the relative importance and directional impact of these two features across various regression models. A general sensitivity analysis

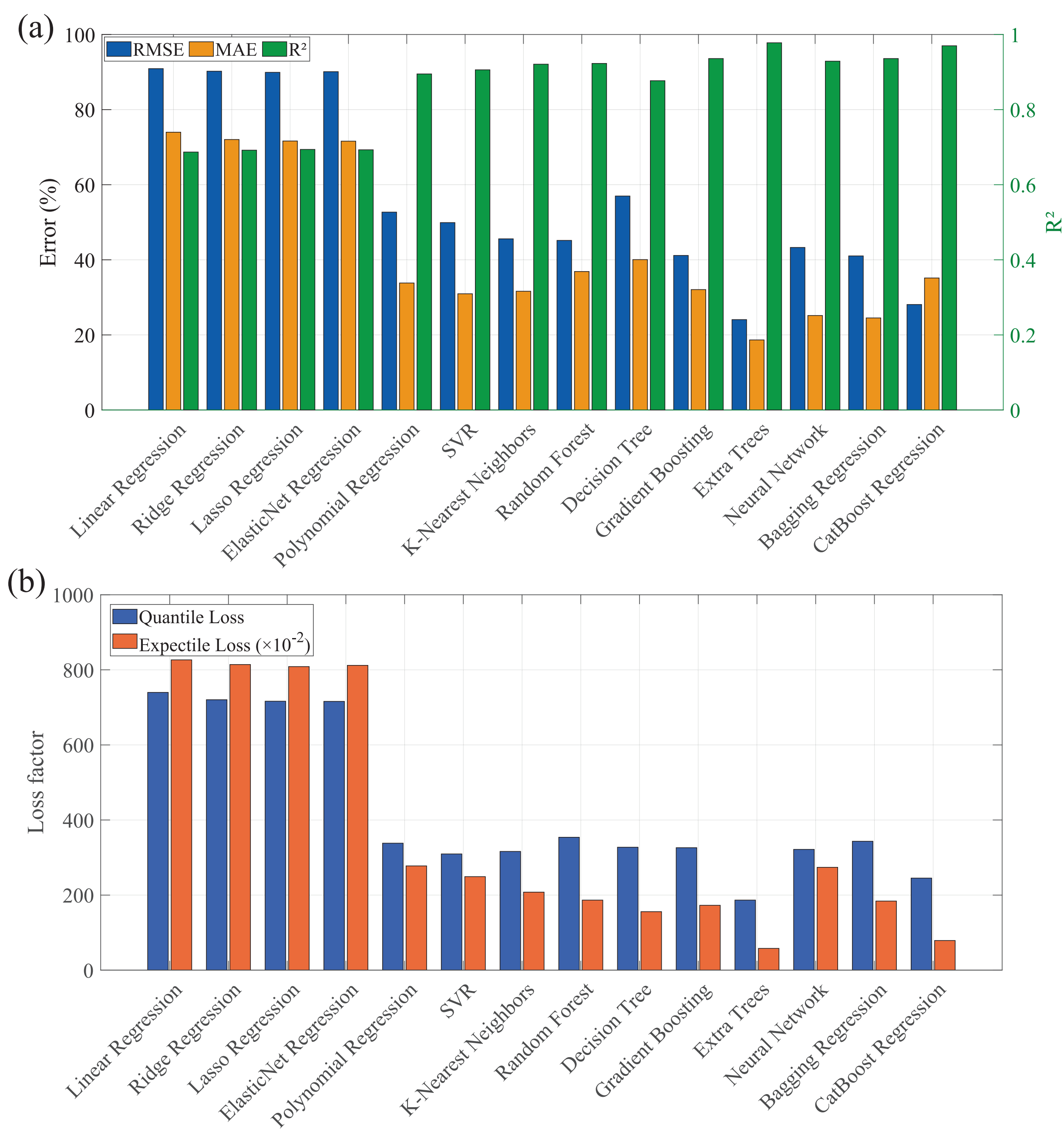

Fig. 6. Performance metrics of ML models. (a) RMSE, MAE, and R^2 shown with dual axes. (b) Quantile and expectile. loss: expectile loss values are scaled by 10^{-2} for visual clarity.

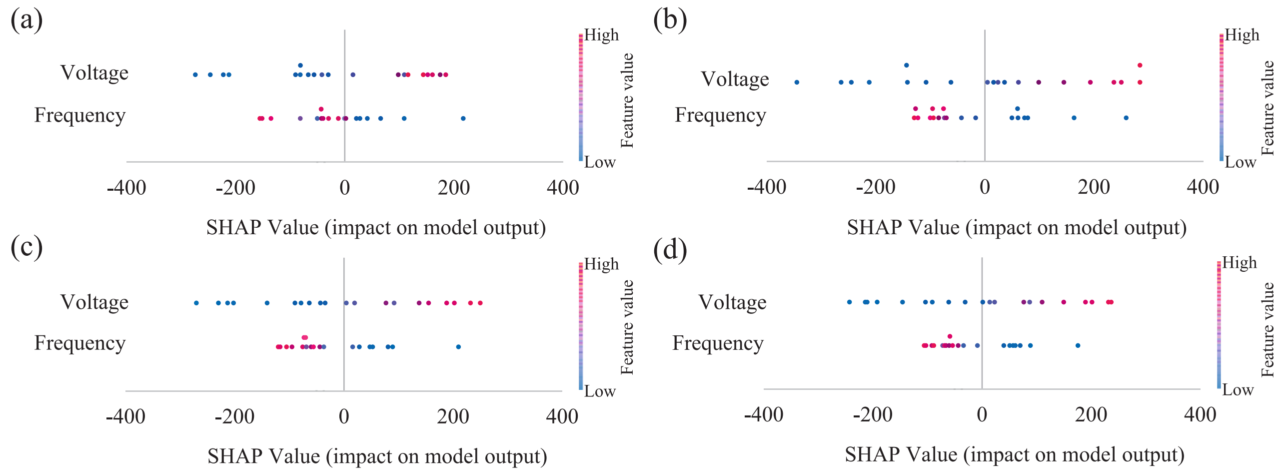

Fig. 7. SHAP value for (a) SVR model, (b) Gradient Boosting model, (c) Extra Trees model and (d) Random Forest model.

confirms that voltage is consistently the dominant feature influencing model outputs, which aligns with expectations since strain is more directly tied to voltage changes in piezoelectric materials. However, frequency also plays a non-negligible role, as each frequency range has a corresponding voltage-strain behaviour due to the dynamic response of the piezoelectric sensors [6]. An additional insight from the SHAP plots is the symmetry in voltage's contribution, suggesting a balanced influence, both positive and negative, across predictions. This reflects the model's ability to adjust to varying strain conditions, making voltage not only the most important feature but also one that contributes robustly to model accuracy. Frequency shows slightly less SHAP variability, but its influence becomes more noticeable in models like Gradient Boosting and Random Forest, which are capable of capturing interactions and non-linearities in the data. This explainability framework provides valuable insight into how the ML models arrive at their predictions, increasing confidence in the model's real-world applicability for SHM.

Fig. 8 illustrates the predicted strain against actual strain plots for selected ML models. These visualisations help assess the predictive accuracy of the chosen models by comparing their outputs with the actual strain values.

The dashed line in each subplot represents the linear trend of the test and train data. Among the models evaluated, the CatBoost Regressor demonstrates the highest accuracy, with predicted values closely aligned with the ideal line and minimal dispersion across both training and test datasets. The Extra Trees Regressor also performs well, though it shows slightly increased scatter, particularly at lower strain levels, indicating a minor tendency toward underfitting in that region. In contrast, the Neural Network model captures the general trend but exhibits greater variability, especially in test data predictions at low strain values, suggesting limited generalisation capability. The Bagging

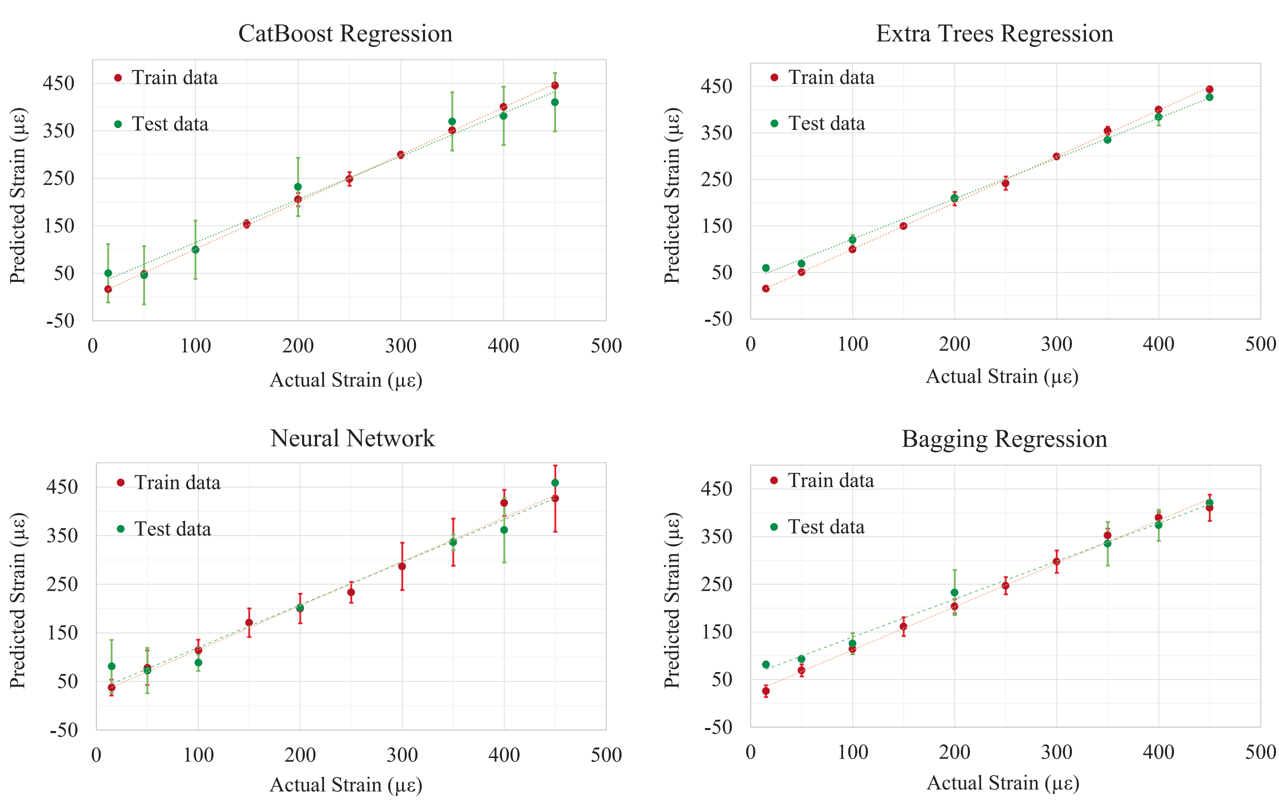

Fig. 8. Predicted strain vs actual strain for four different ML models.

Regressor displays moderate accuracy, with increased spread in predictions and potential signs of overfitting. Overall, the CatBoost and Extra Trees models show superior predictive reliability, while the Neural Network and Bagging models, despite capturing the overall trend, demonstrate higher prediction error and variability, particularly when applied to unseen data.

Although the proposed models demonstrate high predictive accuracy, the current framework provides deterministic predictions without explicit uncertainty quantification. Increased prediction variability is observed at low strain levels, which is attributed to low signal-to-noise ratio (SNR) conditions. This indicates that model reliability may decrease near the lower detection limits of the sensor. Future work will focus on incorporating uncertainty-aware approaches, such as prediction intervals, quantile regression, and Bayesian methods, to better characterise confidence bounds and define operational limits for reliable strain estimation.

In addition, the identification of a minimum reliable strain threshold or SNR-based failure boundary beyond the scope of the present study and was not experimentally established. Establishing such operational limits is important for practical SHM deployment and will be investigated in future work.

The observed scatter in asphalt predictions compared to Teflon can be attributed to the material heterogeneity and non-uniform strain transfer. Asphalt is a heterogeneous composite material, and local variations in aggregate distribution, air void content, and binder stiffness can lead to non-uniform strain fields at the mesoscale. When a surface-mounted PZT sensor is used, the measured response represents an effective, spatially averaged strain over the sensor footprint rather than a point-wise strain value. As a result, local strain concentrations associated with aggregates or voids may not be fully captured, introducing additional variability in the voltage–strain relationship. This heterogeneity-induced variability likely contributes to the increased scatter observed in asphalt predictions compared to the homogeneous Teflon specimen. Importantly, the use of machine-learning-based calibration mitigates this effect by learning an effective mapping between sensor output and global bending-induced strain, rather than relying on an idealized local strain assumption. This observation aligns with the stress–strain validation (Fig. 5), where asphalt showed a steeper, but less uniform response compared to the homogeneous Teflon specimen. Together, these findings highlight that while calibration models trained on Teflon provide transferable accuracy, their performance on asphalt can be influenced by local heterogeneity and bonding conditions.

Overall, Extra Trees Regression and CatBoost Regression achieved the best performance within the adopted validation framework ($R^2 > 0.97$, RMSE < 30 με) and robustness, making them strong candidates for real-time SHM. These models enable accurate strain prediction from minimal inputs (voltage, frequency) and can be integrated into embedded monitoring systems. However, they were trained on Teflon and tested on asphalt in controlled conditions; field deployment may require recalibration to account for environmental effects, mixture variability.

Asphalt is a temperature-sensitive viscoelastic material, and its stiffness and strain response are known to vary with temperature. In this study, temperature was intentionally kept constant to focus on sensor calibration and machine-learning-based signal–strain mapping under controlled dynamic bending conditions. The objective was not to capture temperature-dependent asphalt behaviour, but to establish a robust calibration framework for piezoelectric sensors. The proposed data-driven approach is readily extensible, as temperature can be incorporated as an additional input variable in future multi-temperature datasets, enabling application under realistic field conditions.

5. Conclusions and future work

This study focuses on sensor calibration and strain monitoring using PZT sensors in an asphalt beam. Key experimental variables, such as strain amplitude, loading frequency, and sensor attachment method, were varied to generate a comprehensive dataset. Instead of relying on traditional physics-based calibration, a data-driven approach was adopted: ML techniques with different complexities were applied to experimentally collected sensor data to learn the relationship between voltage output and applied strain at specific frequencies. In the context of this study, *reliable strain monitoring* refers to the consistent and physically interpretable prediction of strain from piezoelectric sensor outputs under varying strain amplitudes and loading frequencies. This reliability is supported by the experimental evaluation of sensor attachment strategies, analysis of signal behaviour across different strain levels, and the use of multiple regression performance metrics together with model interpretability analysis.

- The FA method is a more effective attachment method than the TEA. The FA approach generated more reliable voltage signals that exhibited a clear, nearly linear relationship with the applied strain. In contrast, the TEA method was less successful because it resulted in poor signal transmission, primarily caused by gaps between the sensor and the substrate.
- The results demonstrated that while the piezoelectric sensor reliably detects cyclic strains, noise and high-frequency disturbances are more pronounced at low strain levels due to system inconsistencies. These issues are less significant at higher strains owing to an improved signal-to-noise ratio, highlighting the importance of considering both sensor output magnitude and system stability in the interpretation and calibration of piezoelectric responses.
- Different ML models were used to interpret the sensor data and predict strain. Ensemble models like Extra Trees Regression performed the best, with high accuracy and low errors. SHAP analysis confirmed that voltage was the most important feature influencing the predictions, with frequency also playing a significant role. The predicted strains closely matched the actual values, especially for models like CatBoost Regressor.
- To scale this framework for real-world applications, future work should consider the optimisation of sensor layout across pavement sections. The performance of distributed piezoelectric sensor networks could be simulated to determine optimal sensor spacing, orientation, and depth, maximising data quality while minimising deployment cost. Real-time data collection from sensors installed in test tracks or in-service pavements could enable validation under realistic environmental and loading conditions. Incorporating additional environmental factors, such as temperature, and applying data fusion strategies may further enhance prediction robustness for practical applications.
- While this study focuses on laboratory validation, future work will address practical field implementation of PZT strain sensors in pavements, with particular emphasis on protective housing or encapsulation strategies to mitigate mechanical damage during construction and traffic loading. The proposed calibration framework is independent of the installation method and can be directly extended to field conditions once suitable protection solutions are established.
- The term “real-time” in this study refers to low-latency inference after offline model training. The input feature space is limited (voltage and frequency), enabling computationally efficient predictions even for ensemble models such as Extra Trees and CatBoost. However, no model compression, pruning, or embedded implementation was performed in this work. Future research will investigate lightweight optimisation techniques, including model pruning, quantisation, and deployment on edge devices, to validate real-time performance under practical field conditions.

Declaration of generative AI and AI-assisted technologies in the writing process

During the preparation of this work, the authors used ChatGPT to improve English language and writing clarity. After using this tool, the authors reviewed and edited the content as needed and take full responsibility for the content of the publication.

CRediT authorship contribution statement

Aliakbar Ghaderiaram: Writing – original draft, Visualization, Methodology, Formal analysis, Data curation, Conceptualization. **Ali Golmohammadi:** Writing – original draft, Formal analysis, Data curation. **Erik Eschlangen:** Writing – review & editing, Supervision, Resources. **Mohammad Fotouhi:** Writing – review & editing, Supervision, Resources, Project administration.

Declaration of competing interest

The authors declare that they have no known competing financial interests or personal relationships that could have appeared to influence the work reported in this paper.

Acknowledgements

The authors gratefully acknowledge Delft University of Technology for providing access to the laboratory facilities, instrumentation, and technical assistance required for the experiments. The authors also thank Dura Vermeer for preparing and supplying the asphalt specimens used in this research. The constructive guidance and discussions from colleagues and supervisors, assistance from Syed Baqir Ali Kazmi and Ali Tabatabaeian that contributed significantly to the completion of this work.

Data availability

Data will be made available on request.

References

[1] M. Wu, L. Yin, M. Li, Z. You, D. Jin, K. Xin, A state-of-the-art review of asphalt aging behavior at macro, micro, and molecular scales, Constr. Build. Mater. 460 (2025) 139738, https://doi.org/10.1016/J.CONBUILDMAT.2024.139738.

[2] A. Ghaderiaram, E. Schlangen, M. Fotouhi, Structural Fatigue Life Monitoring with Piezoelectric-Based Sensors: Fundamentals, Current Advances, and Future Directions, Sensors 2025, Vol. 25, Page 334 25 (2025) 334. Doi: 10.3390/S25020334.

[3] P. Jiao, K.J.I. Egbe, Y. Xie, A.M. Nazar, A.H. Alavi, Piezoelectric Sensing Techniques in Structural Health Monitoring: A State-of-the-Art Review, Sensors 2020, Vol. 20, Page 3730 20 (2020) 3730. Doi: 10.3390/S20133730.

[4] R. Gomasa, V. Talakokula, S. Kalyana Rama Jyosyula, T. Bansal, A review on health monitoring of concrete structures using embedded piezoelectric sensor, Constr. Build. Mater. 405 (2023) 133179. Doi: 10.1016/J.CONBUILDMAT.2023.133179.

[5] F. Gulisano, D. Jimenez-Bermejo, S. Castano-Solís, L.A. Sánchez Diez, J. Gallego, Development of Self-Sensing Asphalt Pavements: Review and Perspectives, Sensors 2024, Vol. 24, Page 792 24 (2024) 792. Doi: 10.3390/S24030792.

[6] A. Ghaderiaram, N. Vafa, E. Schlangen, M. Fotouhi, Piezoelectric sensor characterization for structural strain measurements, Sens. Actuators A Phys. 391 (2025) 116659, https://doi.org/10.1016/J.SNA.2025.116659.

[7] J. Sirohi, I. Chopra, Fundamental Understanding of Piezoelectric Strain Sensors (2001), https://doi.org/10.1106/8BFB-GC8P-XQ47-YCQ0.

[8] J. Wang, Y. Han, Z. Cao, X. Xu, J. Zhang, F. Xiao, Applications of optical fiber sensor in pavement Engineering: a review, Constr. Build. Mater. 400 (2023) 132713, https://doi.org/10.1016/J.CONBUILDMAT.2023.132713.

[9] J. Braunfelds, U. Senkans, P. Skels, R. Janeliukstis, J. Porins, S. Spolitis, V. Bobrovs, J. Braunfelds, U. Senkans, P. Skels, R. Janeliukstis, J. Porins, S. Spolitis, V. Bobrovs, Road Pavement Structural Health Monitoring by Embedded Fiber-Bragg-Grating-Based Optical Sensors, Sensors 2022, Vol. 22, 22 (2022). Doi: 10.3390/S22124581.

[10] J.P. Lynch, A Summary Review of Wireless Sensors and Sensor Networks for Structural Health monitoring, the, Shock and Vibration Digest 38 (2006) 91–128, https://doi.org/10.1177/0583102406061499.

[11] G. Han, Y.F. Su, C. Huang, N. Lu, Y. Feng, Field-Validated deep learning model for Piezoelectric-based In-Situ concrete strength sensing, Mech. Syst. Signal Process. 232 (2025) 112768, https://doi.org/10.1016/J.YMSSP.2025.112768.

[12] Y. Wang, J. Li, X. Zhang, Y. Yao, Y. Peng, Recent Development in Intelligent Compaction for Asphalt Pavement Construction: Leveraging Smart Sensors and Machine Learning, Sensors 2024, Vol. 24, Page 2777 24 (2024) 2777. Doi: 10.3390/S24092777.

[13] B. Mourched, M. Hoxha, A. Abdelgalil, N. Ferko, M. Abdallah, A. Potams, A. Lushi, H.I. Turan, S. Vrtagic, Piezoelectric-Based Sensor Concept and Design with Machine Learning-Enabled Using COMSOL Multiphysics, Applied Sciences 2022, Vol. 12, Page 9798 12 (2022) 9798. Doi: 10.3390/APP12199798.

[14] K. Gui, J. Ge, L. Ye, L. Huang, The piezoelectric road status sensor using the frequency scanning method and machine-learning algorithms, Sens. Actuators A Phys. 287 (2019) 8–20, https://doi.org/10.1016/J.SNA.2018.12.048.

[15] M.A. de Oliveira, A. V. Monteiro, J.V. Filho, A New Structural Health Monitoring Strategy Based on PZT Sensors and Convolutional Neural Network, Sensors 2018, Vol. 18, Page 2955 18 (2018) 2955. Doi: 10.3390/S18092955.

[16] E.J. Cross, S.J. Gibson, M.R. Jones, D.J. Pitchforth, S. Zhang, T.J. Rogers, Physics-Informed Machine Learning for Structural Health monitoring, Structural Integrity 21 (2022) 347–367, https://doi.org/10.1007/978-3-030-81716-9_17/FIGURES/9.

[17] C. Xu, X. Chen, Q. Zeng, M. Cai, W. Zhang, B. Yu, A framework of integrating machine learning model and pavement life cycle assessment to optimize asphalt mixture design, Constr. Build. Mater. 469 (2025) 140481, https://doi.org/10.1016/J.CONBUILDMAT.2025.140481.

[18] J. Liu, F. Liu, H. Gong, E.O. Fanijo, L. Wang, Improving asphalt mix design by predicting alligator cracking and longitudinal cracking based on machine learning and dimensionality reduction techniques, Constr. Build. Mater. 354 (2022) 129162, https://doi.org/10.1016/J.CONBUILDMAT.2022.129162.

[19] J. Liu, F. Liu, C. Zheng, E.O. Fanijo, L. Wang, Improving asphalt mix design considering international roughness index of asphalt pavement predicted using autoencoders and machine learning, Constr. Build. Mater. 360 (2022) 129439, https://doi.org/10.1016/J.CONBUILDMAT.2022.129439.

[20] H. Li, R. Nyirandayisabye, Q. Dong, R. Niyirora, T. Hakuzweyezu, I.A. Zardari, F. Nkinahamira, Crack damage prediction of asphalt pavement based on tire noise: a comparison of machine learning algorithms, Constr. Build. Mater. 414 (2024) 134867, https://doi.org/10.1016/J.CONBUILDMAT.2024.134867.

[21] Y. Que, Y. Dai, X. Ji, A. Kwan Leung, Z. Chen, Y. Tang, Z. Jiang, Automatic classification of asphalt pavement cracks using a novel integrated generative adversarial networks and improved VGG model, Eng. Struct. 277 (2023) 115406, https://doi.org/10.1016/J.ENGSTRUCT.2022.115406.

[22] S. Mangalathu, S.H. Hwang, J.S. Jeon, Failure mode and effects analysis of RC members based on machine-learning-based SHapley Additive exPlanations (SHAP) approach, Eng. Struct. 219 (2020) 110927, https://doi.org/10.1016/J.ENGSTRUCT.2020.110927.

[23] A. Hamid, H. Baaj, M. El-Hakim, Temperature and Aging Effects on the Rheological Properties and Performance of Geopolymer-Modified Asphalt Binder and Mixtures, Materials 2023, Vol. 16, Page 1012 16 (2023) 1012. Doi: 10.3390/MA16031012.

[24] K. Diouri, T. El-Korchi, N. Karanjgaokar, R.B. Mallick, Aging and temperature effects on the dynamic characteristics of asphalt mortar under impact loading, Constr. Build. Mater. 369 (2023) 130572, https://doi.org/10.1016/J.CONBUILDMAT.2023.130572.

[25] H. Wei, H. Zhang, J. Li, J. Zheng, J. Ren, Effect of loading rate on failure characteristics of asphalt mixtures using acoustic emission technique, Constr. Build. Mater. 364 (2023) 129835, https://doi.org/10.1016/J.CONBUILDMAT.2022.129835.

[26] A. Ghaderiaram, E. Schlangen, M. Fotouhi, Analysis of PZT Piezoelectric Sensors in Buckling Mode for Dynamic Strain Measurement, (n.d.). Doi: 10.58286/29596.

[27] J. Kim, B.L. Grisso, J.K. Kim, D.S. Ha, D.J. Inman, Electrical modeling of piezoelectric ceramics for analysis and evaluation of sensory systems, 2008 IEEE Sensors Applications Symposium, SAS-2008 - Proceedings (2008) 122–127. Doi: 10.1109/SAS13374.2008.4472956.

[28] J.O. Ogutu, T. Schulz-Streeck, H.P. Piepho, Genomic selection using regularized linear regression models: Ridge regression, lasso, elastic net and their extensions, BMC Proc. 6 (2012) 1–6, https://doi.org/10.1186/1753-6561-6-S2-S10/TABLES/1.

[29] M. Verma, A. Thirumalaiselvi, J. Rajasankar, Kernel-based models for prediction of cement compressive strength, Neural Comput. Appl. 28 (2017) 1083–1100, https://doi.org/10.1007/S00521-016-2419-0/FIGURES/15.

[30] B. Asadi, R. Hajj, Prediction of asphalt binder elastic recovery using tree-based ensemble bagging and boosting models, Constr. Build. Mater. 410 (2024) 134154, https://doi.org/10.1016/J.CONBUILDMAT.2023.134154.

[31] Y. Song, J. Liang, J. Lu, X. Zhao, An efficient instance selection algorithm for k nearest neighbor regression, Neurocomputing 251 (2017) 26–34.

[32] M. Czajkowski, M. Kretowski, The role of decision tree representation in regression problems–an evolutionary perspective, Appl. Soft Comput. 48 (2016) 458–475.

[33] M. Maurizi, C. Gao, F. Berto, Predicting stress, strain and deformation fields in materials and structures with graph neural networks, Scientific Reports 2022 12:1 12 (2022) 1–12. Doi: 10.1038/s41598-022-26424-3.

[34] D.J. Kim, G.W. Kim, J. hyeon Baek, B. Nam, H.S. Kim, Prediction of stress-strain behavior of carbon fabric woven composites by deep neural network, Compos. Struct. 318 (2023) 117073. Doi: 10.1016/J.COMPSTRUCT.2023.117073.

[35] D.E. Hilt, D.W. Seegrist, Ridge, a computer program for calculating ridge regression estimates, Department of Agriculture, Forest Service, Northeastern Forest Experiment … (1977).

[36] R. Tibshirani, Regression shrinkage and selection via the lasso, J. r. Stat. Soc. Series B Stat. Methodol. 58 (1996) 267–288.

[37] Y. Huang, C. Schell, T.B. Huber, A.N. Şimşek, N. Hersch, R. Merkel, G. Gompper, B. Sabass, Traction force microscopy with optimized regularization and automated Bayesian parameter selection for comparing cells, Sci. Rep. 9 (2019) 539.

[38] E. Ostertagová, Modelling using polynomial regression, Procedia Eng. 48 (2012) 500–506.

[39] C. Comito, C. Pizzuti, Artificial intelligence for forecasting and diagnosing COVID-19 pandemic: a focused review, Artif. Intell. Med. 128 (2022) 102286.

[40] P. Srisuradetchai, K. Suksrikran, Random kernel k-nearest neighbors regression, Front. Big Data 7 (2024) 1402384.

[41] K. Tretiak, G. Schollmeyer, S. Ferson, Neural network model for imprecise regression with interval dependent variables, Neural Netw. 161 (2023) 550–564.

[42] P. Jain, A. Choudhury, P. Dutta, K. Kalita, P. Barsocchi, Random forest regression-based machine learning model for accurate estimation of fluid flow in curved pipes, Processes 9 (2021) 2095.

[43] M. Mame, S. Huang, C. Li, J. Zhou, Application of Extra-Trees Regression and Tree-Structured Parzen Estimators Optimization Algorithm to Predict Blast-Induced mean Fragmentation size in Open-pit Mines, Appl. Sci. 15 (2025) 8363.

[44] A. Sharafati, S.B.H.S. Asadollah, N. Al-Ansari, Application of bagging ensemble model for predicting compressive strength of hollow concrete masonry prism, Ain Shams Eng. J. 12 (2021) 3521–3530.

[45] D.A. Otchere, T.O.A. Ganat, J.O. Ojero, B.N. Tackie-Otoo, M.Y. Taki, Application of gradient boosting regression model for the evaluation of feature selection techniques in improving reservoir characterisation predictions, J. Pet. Sci. Eng. 208 (2022) 109244.

[46] Z. Xiong, Y. Cui, Z. Liu, Y. Zhao, M. Hu, J. Hu, Evaluating explorative prediction power of machine learning algorithms for materials discovery using k-fold forward cross-validation, Comput. Mater. Sci 171 (2020) 109203, https://doi.org/10.1016/J.COMMATSCI.2019.109203.

[47] Y. Zhao, W. Zhang, X. Liu, Grid search with a weighted error function: Hyper-parameter optimization for financial time series forecasting, Appl. Soft Comput. 154 (2024) 111362, https://doi.org/10.1016/J.ASOC.2024.111362.

[48] P. Sulejmani, S. Said, S. Agardh, A. Ahmed, Impact of temperature and moisture on the tensile strain of asphalt concrete layers, Int. J. Pavement Eng. 22 (2021) 1711–1719, https://doi.org/10.1080/10298436.2020.1715404.

[49] A.R. Ghanizadeh, M. Fakhri, Prediction of Frequency for simulation of Asphalt Mix Fatigue Tests using MARS and ANN, Scientific World Journal 2014 (2014) 515467, https://doi.org/10.1155/2014/515467.

[50] H. Cheng, Y. Wang, M. Asce, L. Liu, L. Sun, Y. Zhang, R. Yang, Estimating Tensile and Compressive Moduli of Asphalt Mixture from indirect Tensile and Four-Point Bending Tests, J. Mater. Civ. Eng. 33 (2020) 04020402, https://doi.org/10.1061/(ASCE)MT.1943-5533.0003476.

[51] P. Khanal, M. Mamlouk, Tensile versus compressive moduli of asphalt concrete, Transp. Res, Rec, 1995.

[52] A. Golmohammadi, Towards Accurate Road Health Monitoring: A Damage Detection System Using FBG Sensors. https://doi.org/10.3217/978-3-99161-057-1-109.

[53] A. Ghaderiaram, E. Eschlangen, M. Fotouhi, On-Device tilt and symmetry sensing with a MEMS Accelerometer: An Integration-Free embedded approach, Measurement 31 (2026) 120992, https://doi.org/10.1016/j.measurement.2026.120992.

[54] A. Ghaderiaram, E. Schlangen, M. Fotouhi, Piezoelectric sensor characterization in buckling mode for structural dynamic strain measurements, Sensors and Actuators Reports 10 (2025) 100362, https://doi.org/10.1016/j.snr.2025.100362.